Unusual and Highly Tunable Missing-Linker Defects in Zirconium Metal−Organic Framework UiO-66 and Their Important Effects on Gas Adsorption

Hui Wu,[†,‡] Yong Shen Chua,[†,§] Vaiva Krungleviciute,[†,‖] Madhusudan Tyagi,[†,‡] Ping Chen,[§] Taner Yildirim,[†,‖] and Wei Zhou*[,†,‡]

[†]NIST Center for Neutron Research, National Institute of Standards and Technology, Gaithersburg, Maryland 20899-6102, United States

[‡]Department of Materials Science and Engineering, University of Maryland, College Park, Maryland 20742, United States

[§]Dalian Institute of Chemical Physics, Chinese Academy of Sciences, 457# Zhongshan Road 116023, Dalian, China

[‖]Department of Materials Science and Engineering, University of Pennsylvania, Philadelphia, Pennsylvania 19104, United States

S *Supporting Information*

ABSTRACT: UiO-66 is a highly important prototypical zirconium metal−organic framework (MOF) compound because of its excellent stabilities not typically found in common porous MOFs. In its perfect crystal structure, each Zr metal center is fully coordinated by 12 organic linkers to form a highly connected framework. Using high-resolution neutron power diffraction technique, we found the first direct structural evidence showing that real UiO-66 material contains significant amount of missing-linker defects, an unusual phenomenon for MOFs. The concentration of the missing-

0.44 cc/g   1.0 cc/g

Tunable missing linker defects in UiO-66

linker defects is surprisingly high, ∼10% in our sample, effectively reducing the framework connection from 12 to ∼11. We show that by varying the concentration of the acetic acid modulator and the synthesis time, the linker vacancies can be tuned systematically, leading to dramatically enhanced porosity. We obtained samples with pore volumes ranging from 0.44 to 1.0 cm^3/g and Brunauer−Emmett−Teller surface areas ranging from 1000 to 1600 m^2/g, the largest values of which are ∼150% and ∼60% higher than the theoretical values of defect-free UiO-66 crystal, respectively. The linker vacancies also have profound effects on the gas adsorption behaviors of UiO-66, in particular CO_2. Finally, comparing the gas adsorption of hydroxylated and dehydroxylated UiO-66, we found that the former performs systematically better than the latter (particularly for CO_2) suggesting the beneficial effect of the −OH groups. This finding is of great importance because hydroxylated UiO-66 is the practically more relevant, non-air-sensitive form of this MOF. The preferred gas adsorption on the metal center was confirmed by neutron diffraction measurements, and the gas binding strength enhancement by the −OH group was further supported by our first-principles calculations.
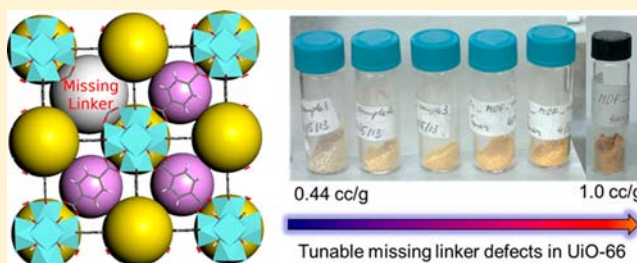
INTRODUCTION

Metal−organic frameworks (MOFs), consisting of inorganic metal centers connected by organic linkers, are a relatively new family of porous materials that possess rich chemistry and offer great promise for gas adsorption related applications.[1−13] Compared to conventional inorganic porous adsorbents (e.g., activated carbon and zeolites), one disadvantage of MOFs is their low thermal, chemical, and mechanical stabilities. Recently, zirconium-based metal−organic frameworks (Zr-MOFs) attracted great attention because of their exceptional stabilities compared to those of other common MOFs.[14−22] They are stable up to 500 °C in air and stable in most chemical solvents. According to calculations, they also possess excellent mechanical stabilities, in particular, high resistance to shear stress to which other MOFs are vulnerable.[23] These attributes

make Zr-MOFs outstanding candidates for practical applications.

UiO-66 is the prototype of this subfamily of MOFs. It has a face-centered-cubic crystal structure, as schematically shown in Figure 1. Each zirconium metal center is connected to 12 benzene-1,4-dicarboxylate (BDC) linkers to form the 3D framework. This high degree of network connection is believed to be the main reason for its high stabilities. Although a perfect UiO-66 crystal has a 12-connected framework structure, recently it was proposed that the real material may contain missing-linker defects, evidenced by thermogravimetric analysis.[24] If such defects exist throughout the UiO-66 structure (though highly uncommon in other MOFs), it would have
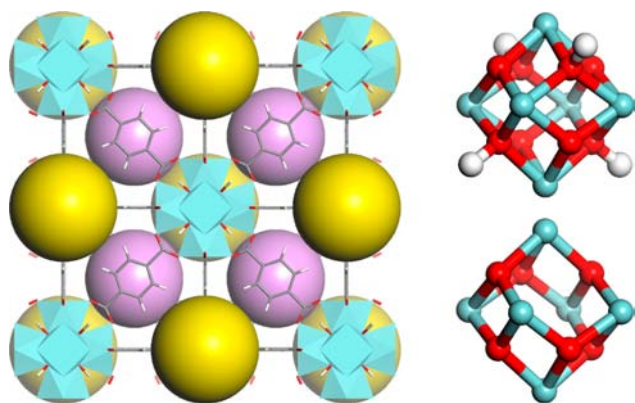
Figure 1. Crystal structure of UiO-66 (hydroxylated form), consisting of Zr−O metal centers connected by BDC linkers. The large yellow and pink spheres represent the two types of pores in this MOF, located at the octahedral sites and the tetrahedral sites, respectively. Zr, cyan; C, gray; O, red; H, white. Shown on the right are the inner core Zr_6-cluster, in hydroxylated form (top) and dehydroxylated form (bottom).

profound consequences, such as weakened structural stabilities due to lowered framework connectivity, and gas adsorption behaviors significantly deviated from those expected for a perfect crystal. Despite the potential importance of this phenomenon, thus far it has not received much attention. This is likely due to two reasons: First, the previous thermogravimetric data suggesting missing-linker defects are not highly convincing because the assumptions used in the data interpretation are not solid,[25] and second, so far there is no direct structural evidence reported to support the existence of the linker vacancies.

In this work, we aimed to address this important issue by performing a series of investigations. We first conducted high-quality neutron diffraction measurements to seek direct structural evidence of missing-linker defects in UiO-66. Next, we investigated the possibilities of systematically tuning the defects and porosities of UiO-66 by varying the synthesis conditions, such as the concentration of acetic acid (AcOH) modulator and the synthesis time. Then, we performed detailed gas adsorption isotherm measurements to examine how significantly the structural vacancies may affect the MOF gas adsorption performance. Finally, we compared fully activated and re-hydroxylated UiO-66 to study the effect of hydroxylation (i.e., the −OH groups coordinated to Zr metal centers) on gas adsorption.

■ RESULTS AND DISCUSSION

1. Direct Structural Evidence of Missing-Linker Defects in UiO-66 from Neutron Diffraction. We start by reviewing the structural information of UiO-66 available in the literature. UiO-66 exists in two different forms. In the as-synthesized material, the Zr ion is 8-coordinated by O, and six of them cluster together forming the $Zr_6O_4(OH)_4$ metal center. Upon full activation at high temperature (~250 °C) in vacuum, each Zr−O cluster loses 2 H_2O molecules, reducing the Zr−O coordination to 7. These two MOF forms were traditionally referred to as the hydroxylated and dehydroxylated UiO-66, respectively. Upon exposing to water vapor in air, the fully dehydroxylated MOF form can readily convert back to the hydroxylated form. The structures of both UiO-66 forms have been extensively studied using X-ray diffraction (XRD)

techniques.[14,24,26] For hydroxylated UiO-66, the structure symmetry was unambiguously identified as $Fm\bar{3}m$. The four −O and four −OH groups within each $Zr_6O_4(OH)_4$ metal center were believed to be ordered (see the schematic in Figure 1) because such arrangement corresponds to the lowest energy configuration. Throughout the lattice, different metal clusters can assume different orientations because they are well-separated (by organic linkers), resulting in random arrangements without long-range order. Therefore, crystallographically, the metal center can be conveniently described as a $Zr_6(OH)_8$ cluster with H being half-occupied. Similarly, in the dehydroxylated UiO-66 structure, the metal center can be described as a Zr_6O_8 clusters with O being 3/4 occupied. Recently, some controversy arose when a synchrotron XRD study suggested that the dehydroxylated UiO-66 can be better described using the $R\bar{3}m$ space group with all Zr_6O_6 clusters oriented in the same direction in the proposed structural model.[26]

To elucidate this controversy and, most importantly, to evaluate whether missing-linker defects indeed pervasively exist in UiO-66, we performed high-resolution neutron power diffraction measurement on a deuterated UiO-66 sample. The sample was synthesized using a "modulator approach" reported in the literature that utilizes acetic acid additive to help improve sample crystallinity,[27] which is beneficial to diffraction studies (sample synthesis details are available in the Supporting Information; also, see Figure S1 for the XRD pattern of the sample). Neutron diffraction is a superb choice compared to XRD in this case because XRD in UiO-66 is dominated by heavy element Zr and not sensitive to the organic linkers because the X-ray scattering cross section of each element is proportional to Z^2 (Z: atomic number). In contrast, neutron diffraction is equally sensitive to the organic linkers and the metal centers in the structure because the coherent neutron scattering cross sections of Zr, O, C, and D are close to each other (6.44, 4.232, 5.551, and 5.592 barns,[28] respectively). Consequently, if linker vacancies indeed exist, neutrons provide much better chance of seeing them than X-rays. Deuteration of the sample is necessary for our measurement in order to greatly eliminate the incoherent scattering background that would otherwise be produced by a regular hydrogenous sample. Such effort ensured that we would obtain high-quality diffraction patterns to pursue the subtle structural information of linker vacancies.

The neutron powder diffraction data that we collected on the fully activated (dehydroxylated), deuterated UiO-66 sample at 4 K are shown in Figure 2 (details of our neutron diffraction experiment are available in the Supporting Information). Additional data were collected at higher temperatures up to 600 K (see Figure S2 for data at 300 K) and also on the hydroxylated sample (see S3). No significant change was observed on the diffraction pattern, suggesting that there is no phase transition in the whole temperature range investigated.

In our data analysis, we considered the two previously proposed structural models for dehydroxylated UiO-66 that are in controversy. We found that our data can be excellently described by a cubic symmetry with no hint of small lattice distortion that would lead to a lower symmetry of $R\bar{3}m$. It is not clear why the $R\bar{3}m$ model seems to work for the data reported in ref 26, but one possibility is due to the low quality of the particular XRD data used (peak positions were artificially affected by the large background in their data refinement.) Thus, we adopted the $Fm\bar{3}m$ model in our structural
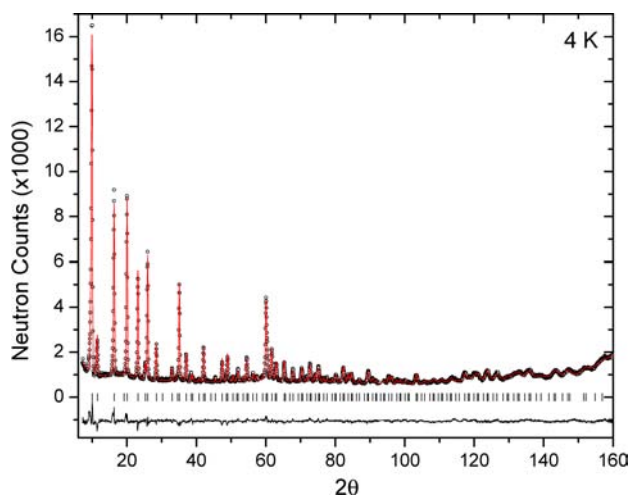
10526

dx.doi.org/10.1021/ja404514r | *J. Am. Chem. Soc.* 2013, 135, 10525−10532

Figure 2. Experimental (circles), calculated (line), and difference (line below observed and calculated patterns) neutron powder diffraction profiles for dehydroxylated, deuterated UiO-66 at 4 K. In our structural model, the missing-linker defects are described by a linker occupancy parameter, the refined value of which is 0.917. Vertical bars indicate the calculated positions of Bragg peaks. Goodness of fit data: $R_{wp} = 0.0452$, $R_p = 0.0364$, $\chi^2 = 1.65$.

refinement. The linker vacancies, if present, would appear in the structure randomly and therefore, could be well-described by a parameter of the linker occupancy. We started our refinement without considering the occupancy of the linker, and were able to obtain a reasonable initial fit (see Figure S4; goodness of fit data: $R_{wp} = 0.0548$, $R_p = 0.0447$, $\chi^2 = 3.430$). We then included the occupancy of the BDC linker $[C_6D_4(CO_2)_2]$ as a free variable in our refinement. We immediately noticed that the quality of the data-fit greatly improved (with difference significantly above the systematic error). As shown in Figure 2, excellent convergence and much-improved goodness-of-fit parameters ($R_{wp} = 0.0452$, $R_p = 0.0364$, $\chi^2 = 1.65$) were obtained in our final refinement. The refined lattice parameters, atomic coordinates, and occupancies are provided in detail in Tables S1 and S2. The refined linker occupancies derived from the 4 and 300 K data are reasonably close, 91.7 and 89.0%, respectively. Note that the refined structure with linkers partially occupied is not charge-neutral. In the real materials, with missing linkers, the positive charges on the metal centers would be balanced by terminal groups (such as −OH groups) at the vacancy sites. We did not explicitly include this effect in our structural model as the chemical composition of the terminal groups is largely unknown. We did test refining the occupancy of only the central section of the linker $[C_6D_4(C)_2]$, instead of the whole linker $[C_6D_4(CO_2)_2]$, with Zr left fully coordinated by O to partially account for the effect of terminal groups. Interestingly, we still obtained similar linker occupancies of 93.8 and 92.4% (from the 4 and 300 K data, respectively), suggesting that the diffraction data and our refinement are not strongly affected by the presumably disordered terminal groups on the defect sites. This provides us further confidence on the validity of our method and the defect concentration that we obtained.

We emphasize that this is the first time that the linker vacancies in UiO-66 have been unambiguously confirmed from structural point of view. This was not possible previously by XRD because X-ray interaction with the sample is dominated by heavy metal Zr and not sensitive to the organic linkers in the

structure, as mentioned earlier. According to our refined linker occupancies, on average, about one out of 12 linkers are missing in UiO-66, effectively reducing the network connection from 12 to 11. Such high concentration of linker vacancies is an unusual phenomenon and was not typically found for other MOFs, which is understandable. In common MOFs, whose inorganic nodes are 4-, 5-, or 6- connected to organic linkers, a missing linker would more likely lead to unstable local framework and pore collapse, resulting in a grain boundary-type defect instead of linker vacancy. The UiO-66 structure intrinsically possesses much better tolerance to missing-linkers due to the much higher network connection without the structural integrity (or "crystallinity") of the 3-D extended framework being disrupted.

2. Highly Tunable Missing-Linker Defects and Their Dramatic Effects on the Porosity of UiO-66. For porous material, higher porosity is generally preferred and beneficial for most applications. Despite the fact that the missing-linkers represent a type of structural "imperfection", one good consequence is boosting the porosity of the MOF material. This concept is essentially the same as the one proposed in a recent theoretical work, where linker removal was suggested as a potential method to increase the MOF pore volume and surface area.[29] Indeed, for a perfect UiO-66 crystal, the theoretical pore volume and surface area are modest: 0.426 cm^3/g and 954 m^2/g, respectively. For a crystal with 1 out of 12 linkers artificially removed for every metal center in the unit cell (i.e., a hypothetic model structure with ordered defects), the calculated values increase significantly to 0.502 cm^3/g and 1433 m^2/g, respectively.

Inspired by this observation, in this section we investigated whether the porosity of UiO-66 can be further enhanced by tuning the missing-linker defects. It is likely that the concentration and morphology of the linker vacancies in UiO-66 material may vary with changing synthesis conditions. Particularly relevant is the "modulator approach", now widely adopted in MOF synthesis, where a monocarboxylic acid was used as an additive to regulate the MOF crystal growth.[30,31] For UiO-66, it has been well-demonstrated that the direct reaction of $ZrCl_4$ with the BDC linker precursor resulted in intergrown aggregates of small crystallites. Adding acetic acid as a modulator helps MOF crystal growth and leads to significantly larger crystals with well-defined octahedral shape.[27] We expected that by varying the concentration of acetic acid modulator used in the synthesis, it might be possible to systematically tune the defects and the pore volume. We conducted such a study (see Supporting Information for sample synthesis details and Figure S6 for XRD patterns), and the N_2 adsorption isotherms of several samples at 77 K are shown in Figure 3. Details of gas adsorption measurement are provided in Supporting Information, and all isotherms are also plotted in semi-log scale in Figure S7 in order to show the adsorption at low pressure more clearly. Pore volumes derived from the N_2 isotherms based on the Dubinin−Radushkevich method and the nonlocal density functional theory (NLDFT) model are provided in Table S4. Pore size distributions were also derived using NLDFT model for these samples, and compared with the geometric pore size distributions for the ideal UiO-66 structure and two hypothetic structures with ordered missing-linker defects (see Figures S14 and S15). We found that by increasing the amount of acetic acid used in the synthesis, the pore volume can be systematically tuned from the no-AcOH limit of 0.44 cm^3/g to up to 0.65 cm^3/g (∼50% higher than the calculated
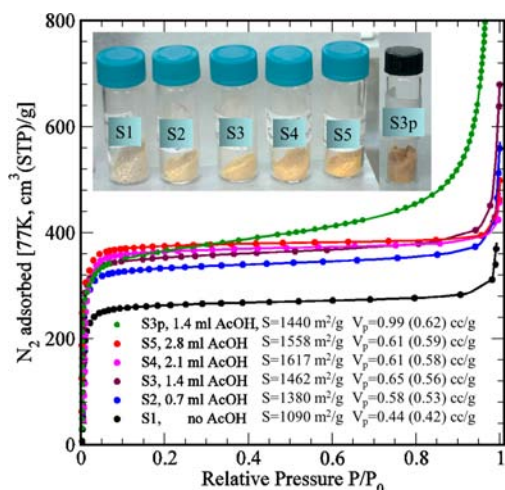
Figure 3. N$_2$ adsorption isotherms at 77 K of several UiO-66 samples synthesized using different amounts of acetic acid modulator. All samples were fully activated/dehydroxylated before measuring. The inset shows the picture of the actual samples with colors varying from white to yellow to brown with increasing amount of defects. The BET surface area (S) and the total pore volumes (V_p, calculated on the basis of N$_2$ density of 34.7 cm^3/mmol at 77 K) for each sample are also shown. The numbers in parentheses are micropore volumes derived using the Dubinin−Radushkevich method. The individual isotherms, along with the consistency and BET plots, are given in Figures S8−S13.

Figure 4. Neutron inelastic spectrum of UiO-66 measured at 1.5 K using a Neutron Disk−Chopper Spectrometer. The two tunneling peaks (denoted by arrows) are signatures of −CH$_3$ groups. The relatively high tunneling energies (±0.400 meV) imply a low rotational barrier (5.04 meV), consistent with the fact that the methyl groups terminating the defects sites would point to the pore space and are thus rotationally quasi-free.

value of perfect UiO-66 structure). Similarly, we observed the BET surface area increases systematically from the no-AcOH limit of 1000 m^2/g to 1620 m^2/g (~60% higher than the calculated value of perfect UiO-66 structure). For one sample (Figure S3), we also extended the synthesis time from 1 day to 2 days to generate an additional sample (S3p). We found that by increasing the synthesis time, the pore volume is further increased to 1.0 cm^3/g. However, longer synthesis time also leads to larger deviation of the isotherm type from type-I toward type-II, which suggests increasing amounts of mesopores. Interestingly, the samples also exhibit a color change (see the inset of Figure 3) with increasing porosities. This suggests that missing-linker defects might also have changed the electronic band structures of UiO-66 to certain extent. We are in the process of understanding this phenomenon and will publish our findings in due course.

The fact that acetic acid additives greatly enhance UiO-66 porosity made us wonder whether acetic acid is playing a role more than just providing intermediate reactant and "modulating" the formation of the MOF crystal. In particular, is it possible that acetate groups are actually "promoting" the defect formation during UiO-66 crystal growth by terminating some of the Zr metal centers which directly results in missing framework linkage? To examine this possibility, we performed neutron inelastic scattering measurement to look for evidence of methyl groups presenting in our UiO-66 sample (FT-IR measurement was also performed to look for methyl signature, but no clear evidence was obtained, as shown in Figure S16). Neutron spectroscopy is an ideal tool for this purpose. If the methyl groups are terminating some of the missing-linker defects, then we would observe the ground-state tunneling of a quasi-free methyl rotation because the methyl groups pointing toward the pores in the structure should have rather small rotational barriers.[32,33] In Figure 4 we show the neutron
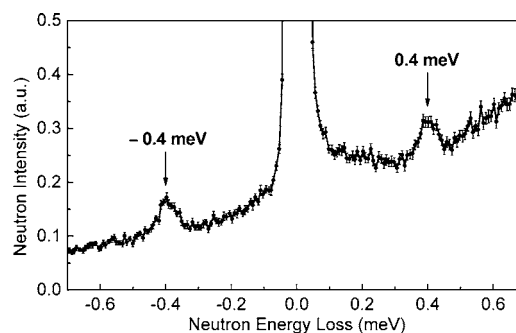
inelastic spectrum of our deuterated UiO-66 sample (the one used in our neutron powder diffraction experiment), measured at 1.5 K using a Disk−Chopper Spectrometer[34] (see measurement details in Supporting Information). The linker deuteration of the sample effectively reduced the interference of low-energy framework vibrational modes (note that only the methyl groups are not deuterated because normal hydrogenated acetic acid was used in the sample synthesis). Two tunneling peaks at ±0.400 meV are apparent and represent signatures of −CH$_3$ groups with rather low rotational barriers (~5.04 meV, see Supporting Information for derivation details).

The neutron inelastic spectrum clearly shows the amount of methyl groups in the sample is significant enough to be detected and at least some of the defect sites are terminated by acetate, although it does not provide quantitative information on the −CH$_3$ concentration in the sample. Thus, we confirmed that the role of acetic acid modulator in Zr-MOF is not only "modulating" the crystal growth, but also participating in the framework formation and promoting "defects". This is in sharp contrast with the modulated synthesis of other MOFs (such as HKUST-1), where it was found that the modulator does not induce significant defects within the framework.[30] This is easily understandable because missing-linker defects are intrinsically unstable in common MOFs with low network connections, as discussed earlier. Interestingly, the role of acetic acid in the modulated synthesis of UiO-66 shares the same spirit as the recently reported, novel approach of MOF synthesis called "metal-ligand-fragment coassembly",[35] where a ligand and a ligand fragment (with pre-designed functional groups) co-assemble with the metal centers and lead to functionalized mesopores. Besides acting as a modulator, the acetic acid in the UiO-66 synthesis also plays a role similar to "ligand-fragment" in an unanticipated way. At this point, it is not clear exactly how the acetic acid affects the morphology of the missing-linker defects in the sample. We speculate that when a larger amount of acetic acid is used, the MOF crystal tends to form a larger quantity and size of internal voids, possibly ranging from several nanometers to tens of nanometers (i.e., mesopores), with metal centers on the mesopore surface partially terminated by acetate. This is consistent with N$_2$ adsorption isotherm data of S3p, which shows an increasing amount of mesopores with increasing synthesis time with the acetic acid used. This also means that the seemingly large, well-shaped octahedral crystals

obtained from a modulator-aided synthesis are not as structurally perfect as they appear.

High concentration of missing-linker defects in UiO-66 is unusual for MOFs. Therefore, to investigate how these vacancies may affect the gas adsorption behaviors would be highly interesting. Figure 5 shows the excess CO_2 and CH_4
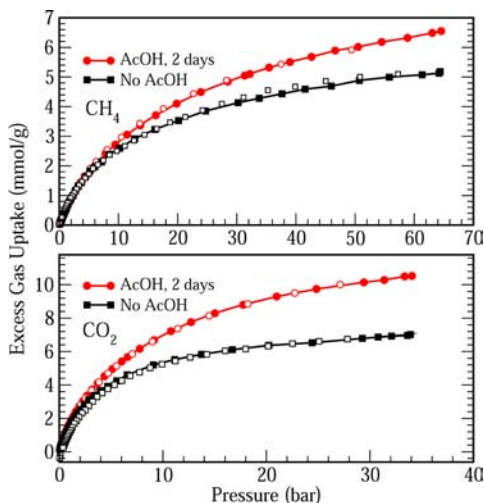

Figure 5. Excess CH_4 (top) and CO_2 (bottom) adsorption isotherms of dehydroxylated UiO-66 samples, synthesized without any AcOH (sample S1) and with AcOH for 2 days (sample S3p).

isotherms for two extreme ends, namely the sample with the least defects (S1) and the one with the most defects (S3p). For the methane isotherm at low pressure, the sample with the most defects shows only 0.25% higher uptake than that of the sample with the least defects. The difference becomes rather significant at high pressures, reaching ~30% at 60 bar. A similar trend is observed for CO_2, with even more dramatic gas uptake enhancement with increased defect concentration. The CO_2 isotherm at low pressure (near 1 bar) is about 10% higher for the sample with the most defects than that of the sample with the least defects. The difference reaches ~50% at 35 bar, again indicating the importance of the large pore and surface area for high-pressure gas adsorption applications. Similar results are also observed for the absolute adsorption isotherms (see Figure S17).

3. Beneficial Effect of the −OH Groups on Gas Binding in UiO-66. The two forms of UiO-66 provide an excellent opportunity to study the effect of −OH groups on pore volume, surface area, and most importantly, gas adsorption because the major difference between the two structures is the −OH groups coordinated to the Zr metal centers. We report detailed isotherm studies of N_2, CH_4, and CO_2 adsorption to compare hydroxylated and dehydroxylated UiO-66. The measurements were done in a broad pressure range using a fully computer-controlled Sieverts-type apparatus.[36] To eliminate sample differences (particularly defect concentrations) in different batches, we used a hydrogenated equivalent of our neutron sample in all the gas adsorption measurements discussed in this section because the defect concentration of this sample was well-characterized by neutron diffraction. Special care was given to the preparation of the hydroxylated sample (see Supporting Information for details). Briefly, we adopted an approach of re-hydroxylation of a fully activated sample, then degassed it at room temperature to remove free

water molecules, which we found generated a cleaner and more reproducible hydroxylated sample than the literature method.[37]

Figure 6 shows the experimental N_2 adsorption isotherms at 77 K (see Figure S19 for N_2 data at 300 K). The derived
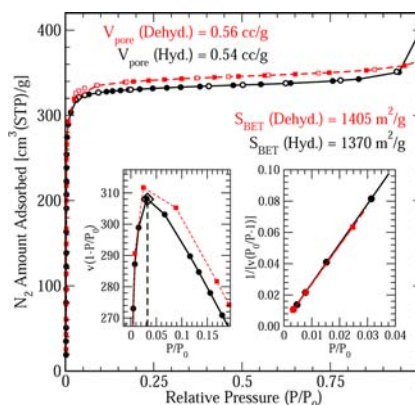

Figure 6. N_2 adsorption isotherms of UiO-66 at 77 K for hydroxylated (black) and dehydroxylated (red) forms. Solid symbols indicate adsorption, whereas open symbols indicate desorption. The insets show the consistency plot (left) and the BET-fitting (right), respectively. The isotherms are also presented in semi-log scale in Figure S18 to show the adsorption at low pressure more clearly.

specific pore volumes are 0.56 and 0.54 cm^3/g, and the derived BET surface areas are 1405 and 1370 m^2/g, for dehydroxylated and hydroxylated UiO-66 samples. The hydroxylated form has slightly lower pore volume and surface area than the dehydroxylated form. This is as expected since the −OH groups are known to simultaneously reduce the pore space in the structure briefly, and increase the crystal density slightly.

In Figure 7, we show the CH_4 and CO_2 excess adsorption isotherms at various temperatures (absolute adsorption isotherms are provided in Figure S20, and CH_4 data are also plotted in semi-log scale in Figure S21 to show the gas uptake in the low-pressure region). It can be clearly seen that the hydroxylated UiO-66 performs systematically better than the dehydroxylated form, despite its slightly smaller pore volume and surface area. For CH_4, the difference is relatively small, while for CO_2, the difference is more prominent, particularly in the low pressure range (see the inset of Figure 7b). At 300 K and 1 bar, the CO_2 uptake in the hydroxylated MOF (2.50 mmol/g) is more than 50% higher than that in the dehydroxylated MOF (1.60 mmol/g).

In Figure 8, we show the isosteric heats of adsorption (Q_{st}) of CH_4 and CO_2, derived from the absolute isotherms at 240, 270, and 300 K, using the virial method. The details and fitting results are given in the Supporting Information (Figures S22 and S23). For CH_4, the Q_{st} of hydroxylated UiO-66 is only slightly higher than (by ~6%) that of the dehydroxylated version, consistent with the small difference in gas uptake amount. In contrast, the initial Q_{st} (at zero coverage) of CO_2, ~28 kJ/mol, found in the former is significantly higher (by ~30%) than that of the latter, ~22 kJ/mol.

In order to attribute the Q_{st} difference to different gas binding energies on the two types of Zr metal centers (with and without −OH groups), we need to confirm that the metal centers are the primary gas adsorption sites in UiO-66. Therefore, we performed neutron diffraction measurements on a hydroxylated UiO-66 sample with adsorbed gas molecules (see Supporting Information for experimental details). The data
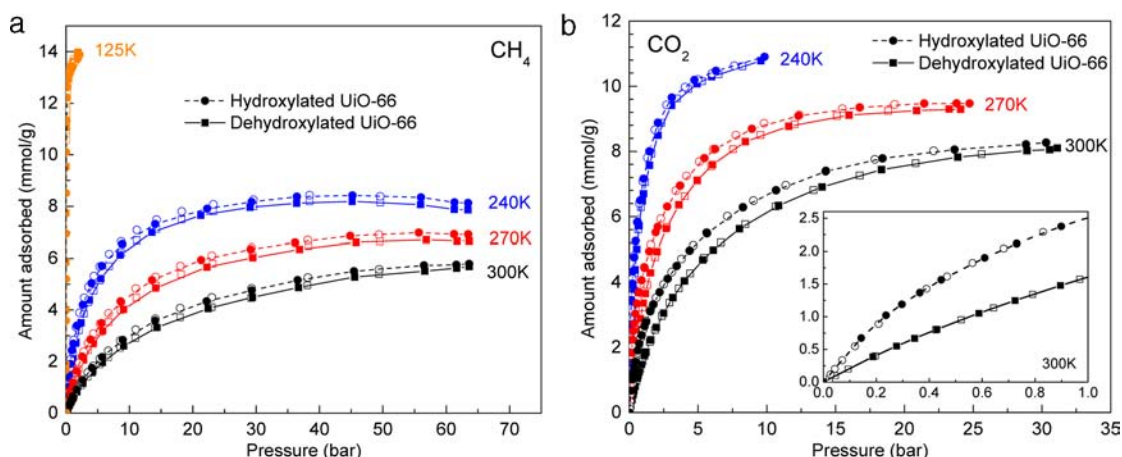
Figure 7. Excess (a) CH_4 and (b) CO_2 adsorption isotherms of hydroxylated and dehydroxylated UiO-66 samples at various temperatures. Solid symbols indicate adsorption, whereas open symbols indicate desorption. The inset on the right shows the low-pressure range for CO_2 adsorption.
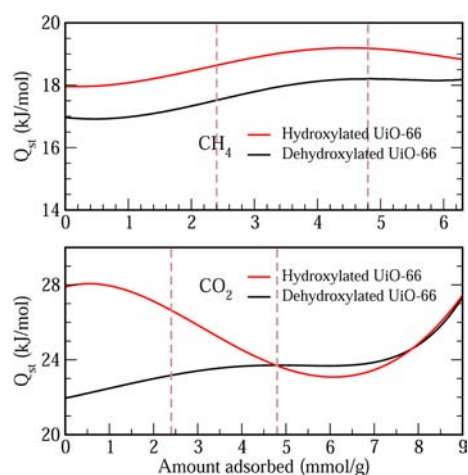

Figure 8. Isosteric heats of adsorption of CH_4 (top) and CO_2 (bottom) in UiO-66. The two vertical dashed-lines indicate the levels of gas-loading when half and all of the eight adsorption sites at each $Zr_6O_4(OH)_4$ metal center are occupied, respectively.

are shown in Figure 9 for CD_4 and CO_2. We found that the gas molecules are indeed preferentially adsorbed at the "cup" sites of Zr metal centers, similar to the case of other MOFs with BDC linkers, such as the well-known MOF-5 $[Zn_4O(BDC)_3]$.[38] Refined gas molecular coordinates are shown in Figure 9 inset, and schematics showing the gas binding positions and orientations are provided in Figure S26. Note that as the diffraction data gave structural average information, it is not possible to tell whether the gas molecules are populated more on the −OH groups than on the −O groups of the metal center or not. Consequently, we used only one set of gas molecule coordinates in our data analysis and were still able to achieve reasonably good refinement.

To further help understand the enhanced gas binding on the hydroxylated UiO-66 sample compared to the dehydroxylated sample, we performed dispersion-corrected density functional theory (DFT-D) calculations[39] (see Supporting Information for details) to derive the static gas binding energies (E_B) on the metal centers. In the hydroxylated form, eight "surfaces" of the Zr_8 octahedral metal center are capped with four −O and four −OH groups, while in the dehydroxylated form, six of them are capped with −O groups and two are uncapped. Thus, there are
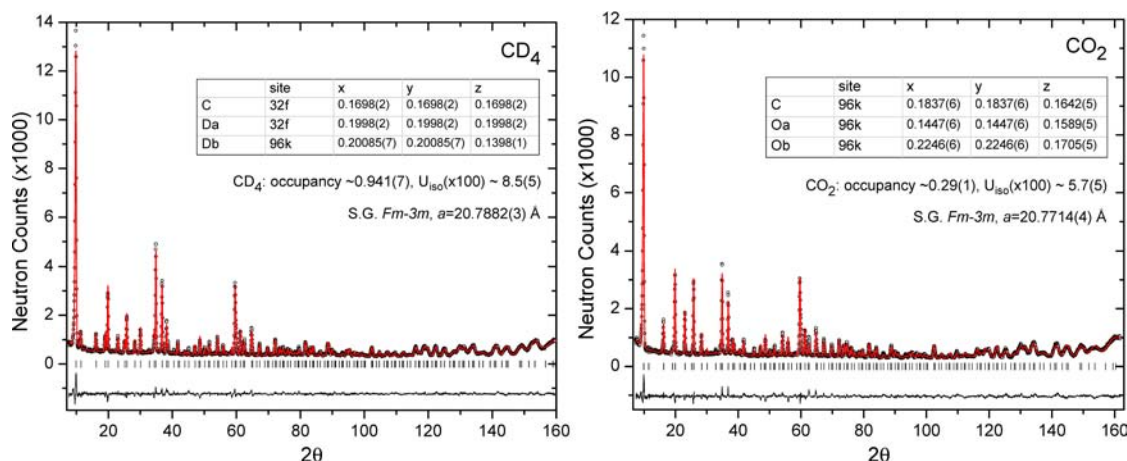

Figure 9. Experimental (circles), calculated (line), and difference (line below observed and calculated patterns) neutron powder diffraction profiles for hydroxylated, deuterated UiO-66 loaded with (left) CD_4 and (right) CO_2, measured at 6 K. Linker occupancy was fixed at 0.92 (the refined value of the bare MOF material). CD_4/CO_2 molecule was kept as rigid body during refinement. Vertical bars indicate the calculated positions of Bragg peaks. Goodness of fit data are CD_4: $R_{wp} = 0.0582$, $R_p = 0.0469$, $\chi^2 = 1.980$; CO_2: $R_{wp} = 0.0671$, $R_p = 0.0522$, $\chi^2 = 2.362$.

three types of adsorption sites on the Zr metal center, and we name them after their capping chemical groups as the " −OH site", the " −O site", and the "void site". The DFT-D optimized CH_4 and CO_2 adsorption configurations and corresponding E_B values at the three different sites are shown in Figure 10. It is
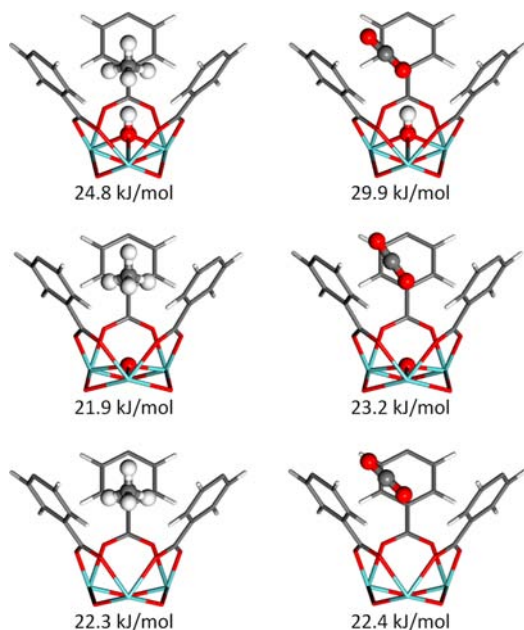

Figure 10. DFT-D optimized CH_4 (left) and CO_2 (right) adsorption configurations on the three different sites of the Zr metal center in UiO-66 (from top to bottom: the −OH site, the −O site, and the void site). The static binding energies are also shown.

clear that the calculated gas binding strengths on the −OH site are higher than those on the −O site and the void site, and the difference is particularly significant for CO_2. This is consistent with the experimental observations. We believe that the enhanced affinity of CO_2 on the −OH site is most likely due to the Columbic interactions between the negatively charged O (of CO_2) and the positively charged H (of the −OH group).

SUMMARY

In this work, we reported the first direct structural evidence for the existence of linker vacancies in UiO-66, obtained from high-resolution neutron power diffraction measurement. The existence of missing-linker defects leads to greatly improved porosity in the real material, and strongly affects its gas adsorption behavior. We found that the acetic acid modulator widely used in the Zr-MOF synthesis promotes the formation of defects and mesopores in a systematic way, yielding dramatic increase in both pore volume and surface area (up to ~150% and ~60%, respectively). Finally, we showed that the −OH groups coordinated to Zr are particularly beneficial to CO_2 adsorption. Note that hydroxylated UiO-66 is the practically more important, non-air-sensitive form of this MOF, whereas the dehydroxylated variant is the activated and air-sensitive form. For typical MOFs, the fully activated, air-sensitive forms usually exhibit better gas affinities and gas uptakes. The fact that air-stable hydroxylated UiO-66 is the better performer makes it even more attractive for practical applications. These findings reported here are likely general to the large family of UiO-66-based Zr-MOFs as they all share the same metal centers and reticular chemistry.

ASSOCIATED CONTENT

S **Supporting Information**

Details of our sample synthesis, neutron diffraction measurement, gas adsorption measurement, neutron inelastic scattering measurement, and first-principle calculations; additional neutron diffraction data and structural parameters obtained from the diffraction data refinement; 77 K N_2 adsorption isotherms, consistency, and BET plots; excess and absolute N_2 and H_2 adsorption isotherms at 300 K; absolute adsorption isotherms of CH_4 and CO_2 at various temperatures; isotherm data plotted in semi-log scale; details of isosteric heat of adsorption plots and virial fits. This material is available free of charge via the Internet at http://pubs.acs.org.

AUTHOR INFORMATION

Corresponding Author

wzhou@nist.gov

Notes

The authors declare no competing financial interest.

ACKNOWLEDGMENTS

REFERENCES

(1) Yaghi, O. M.; O'Keeffe, M.; Ockwig, N. W.; Chae, H. K.; Eddaoudi, M.; Kim, J. *Nature* **2003**, *423*, 705−714.
(2) Kitagawa, S.; Kitaura, R.; Noro, S.-i. *Angew. Chem., Int. Ed.* **2004**, *43*, 2334−2375.
(3) Férey, G. *Chem. Soc. Rev.* **2008**, *37*, 191−214.
(4) Zhou, H.-C.; Long, J. R.; Yaghi, O. M. *Chem. Rev.* **2012**, *112*, 673−674.
(5) Murray, L. J.; Dincă, M.; Long, J. R. *Chem. Soc. Rev.* **2009**, *38*, 1294−1314.
(6) Sculley, J.; Yuan, D.; Zhou, H.-C. *Energy Environ. Sci.* **2011**, *4*, 2721−2735.
(7) Li, J.-R.; Kuppler, R. J.; Zhou, H.-C. *Chem. Soc. Rev.* **2009**, *38*, 1477−1504.
(8) Chen, B.; Xiang, S.; Qian, G. *Acc. Chem. Res.* **2010**, *43*, 1115−1124.
(9) Zhou, W. *Chem. Rec.* **2010**, *10*, 200−204.
(10) Makal, T. A.; Li, J.-R.; Lu, W.; Zhou, H.-C. *Chem. Soc. Rev.* **2012**, *41*, 7761−7779.
(11) He, Y.; Zhou, W.; Krishna, R.; Chen, B. *Chem. Commun.* **2012**, *48*, 11813−11831.
(12) Lee, J.; Farha, O. K.; Roberts, J.; Scheidt, K. A.; Nguyen, S. T.; Hupp, J. T. *Chem. Soc. Rev.* **2009**, *38*, 1450−1459.
(13) Ma, L.; Abney, C.; Lin, W. *Chem. Soc. Rev.* **2009**, *38*, 1248−1256.
(14) Cavka, J. H.; Jakobsen, S.; Olsbye, U.; Guillou, N.; Lamberti, C.; Bordiga, S.; Lillerud, K. P. *J. Am. Chem. Soc.* **2008**, *130*, 13850−13851.
(15) Kandiah, M.; Nilsen, M. H.; Usseglio, S.; Jakobsen, S.; Olsbye, U.; Tilset, M.; Larabi, C.; Quadrelli, E. A.; Bonino, F.; Lillerud, K. P. *Chem. Mater.* **2010**, *22*, 6632−6640.
(16) Garibay, S. J.; Cohen, S. M. *Chem. Commun.* **2010**, *46*, 7700−7702.
(17) Morris, W.; Doonan, C. J.; Yaghi, O. M. *Inorg Chem.* **2011**, *50*, 6853−6855.

(18) Jiang, H.-L.; Feng, D.; Liu, T.-F.; Li, J.-R.; Zhou, H.-C. *J. Am. Chem. Soc.* **2012**, *134*, 14690−14693.

(19) Foo, M. L.; Horike, S.; Fukushima, T.; Hijikata, Y.; Kubota, Y.; Takata, M.; Kitagawa, S. *Dalton Trans.* **2012**, *41*, 13791−13794.

(20) Guillerm, V.; Ragon, F.; Dan-Hardi, M.; Devic, T.; Vishnuvarthan, M.; Campo, B.; Vimont, A.; Clet, G.; Yang, Q.; Maurin, G.; Férey, G.; Vittadini, A.; Gross, S.; Serre, C. *Angew. Chem., Int. Ed.* **2012**, *51*, 9267.

(21) Yang, Q.; Jobic, H.; Salles, F.; Kolokolov, D.; Guillerm, V.; Serre, C.; Maurin, G. *Chem.—Eur. J.* **2011**, *17*, 8882−8889.

(22) Kim, M.; Cahill, J. F.; Fei, H.; Prather, K. A.; Cohen, S. M. *J. Am. Chem. Soc.* **2012**, *134*, 18082−18088.

(23) Wu, H.; Yildirim, T.; Zhou, W. *J. Phys. Chem. Lett.* **2013**, *4*, 925−930.

(24) Valenzano, L.; Civalleri, B.; Chavan, S.; Bordiga, S.; Nilsen, M. H.; Jakobsen, S.; Lillerud, K. P.; Lamberti, C. *Chem. Mater.* **2011**, *23*, 1700−1718.

(25) In ref 24, to derive the concentrations of missing linkers quantitatively, two major assumptions were made: the samples are of pure phase UiO-66, with no impurities such as ZrO_2; and the TGA product at 550 °C is pure ZrO_2. Based on these assumptions, missing-linker concentrations ranging from 8% to 50% were obtained for samples synthesized using same protocol but in different batches. Using the synthesis method in ref 22, we prepared several batches of samples and found that the pore volumes of the activated samples are always ∼0.44 cm^3/g, very close to the theoretical value of a perfect UiO-66 sample, suggesting the defect concentrations are quite low in these materials. We believe that the assumptions used in ref 24 for TGA data analysis are problematic and resulted in misinterpretations.

(26) Wiersum, A. D.; Soubeyrand-Lenoir, E.; Yang, Q.; Moulin, B.; Guillerm, V.; Yahia, M. B.; Bourrelly, S.; Vimont, A.; Miller, S.; Vagner, C.; Daturi, M.; Clet, G.; Serre, C.; Maurin, G.; Llewellyn, P. L. *Chem. Asian J.* **2011**, *6*, 3270−3280.

(27) Schaate, A.; Roy, P.; Godt, A.; Lippke, J.; Waltz, F.; Wiebcke, M.; Behrens, P. *Chem.—Eur. J.* **2011**, *17*, 6643−6651.

(28) Sears, V. F. *Neutron News* **1992**, *3*, 29−37.

(29) Sarkisov, L.; Harrison, A. *Mol. Simul.* **2011**, *37*, 1248−1257.

(30) Diring, S.; Furukawa, S.; Takashima, Y.; Tsuruoka, T.; Kitagawa, S. *Chem. Mater.* **2010**, *22*, 4531−4538.

(31) Tsuruoka, T.; Furukawa, S.; Takashima, Y.; Yoshida, K.; Isoda, S.; Kitagawa, S. *Angew. Chem., Int. Ed.* **2009**, *48*, 4739−4743.

(32) Zhou, W.; Wu, H.; Udovic, T. J.; Rush, J. J.; Yildirim, T. *J. Phys. Chem. A* **2008**, *112*, 12602−12606.

(33) Press, W. Single Particle Rotations in Molecular Crystals, *Springer Tracts in Modern Physics* Vol. 92, Springer: Berlin, 1981.

(34) Copley, J. R. D.; Cook, J. C. *Chem. Phys.* **2003**, *292*, 477.

(35) Park, J.; Wang, Z. U.; Sun, L.-B.; Chen, Y.-P.; Zhou, H.-C. *J. Am. Chem. Soc.* **2012**, *134*, 20110−20116.

(36) Zhou, W.; Wu, H.; Hartman, M. R.; Yildirim, T. *J. Phys. Chem. C* **2007**, *111*, 16131−16137.

(37) In the literature, a hydroxylated UiO-66 sample was usually directly obtained from the solvent-exchanged as-synthesized material by degassing it at a temperature below 100 °C. This process often leads to material with trapped solvent residue or partial dehydroxylation, and thus is poorly reproducible.

(38) Yildirim, T.; Hartman, M. R. *Phys. Rev. Lett.* **2005**, *95*, 215504−215507.

(39) Giannozzi, P.; Baroni, S.; Bonini, N.; Calandra, M.; Car, R.; Cavazzoni, C.; Ceresoli, D.; Chiarotti, G. L.; Cococcioni, M.; Dabo, I.; Dal Corso, A.; Fabris, S.; Fratesi, G.; de Gironcoli, S.; Gebauer, R.; Gerstmann, U.; Gougoussis, C.; Kokalj, A.; Lazzeri, M.; Martin-Samos, L.; Marzari, N.; Mauri, F.; Mazzarello, R.; Paolini, S.; Pasquarello, A.; Paulatto, L.; Sbraccia, C.; Scandolo, S.; Sclauzero, G.; Seitsonen, A. P.; Smogunov, A.; Umari, P.; Wentzcovitch, R. M. *J. Phys.: Condens. Matter* **2009**, *21*, 395502.